

## Chapter 4

### Energy bandwidths of the harmonics

The energy bandwidths of the generated harmonic light will ultimately determine the resolution of the photoelectron spectra obtained, as discussed in chapter 2. High resolution cannot be expected with an ultrafast source, due to the short pulse length and consequent large frequency bandwidth of the laser. However, moderate resolution is needed to observe not only energy splittings in static photoelectron spectra of atoms and molecules, but also to resolve chemical shifts when using the harmonics for pump probe spectroscopy. Therefore, a systematic study of the bandwidths of the harmonics generated in neon was accomplished, as is described here.

The energy widths of low energy photoelectron peaks (below 3 eV) result from the energy width of the harmonic used to ionize the sample. This is demonstrated in Fig. 4.1, where the same spectrum of NO gas taken with a narrowband Nd:YAG laser (10.5 eV) and with the 7th harmonic of the Ti:Sapphire laser (10.85 eV) are overlaid. The dotted line in this figure is the same as in Fig. 2.11, showing the inherent resolution of the magnetic bottle spectrometer. The solid line, resulting from ionization with the 7th harmonic of the Ti:Sapphire laser, demonstrates the broadening of the photoelectron peaks due to the energy bandwidth of the 7th harmonic.

The  $\Delta E_{pe}/E_{pe}$  for any magnetic bottle system is approximately a constant number with  $E_{pe}$  [35], therefore limiting the useful energy range over which bandwidth information of the light source can be obtained. For example, for a  $\Delta E_{pe}/E_{pe}$  of 5% there is already a spec-

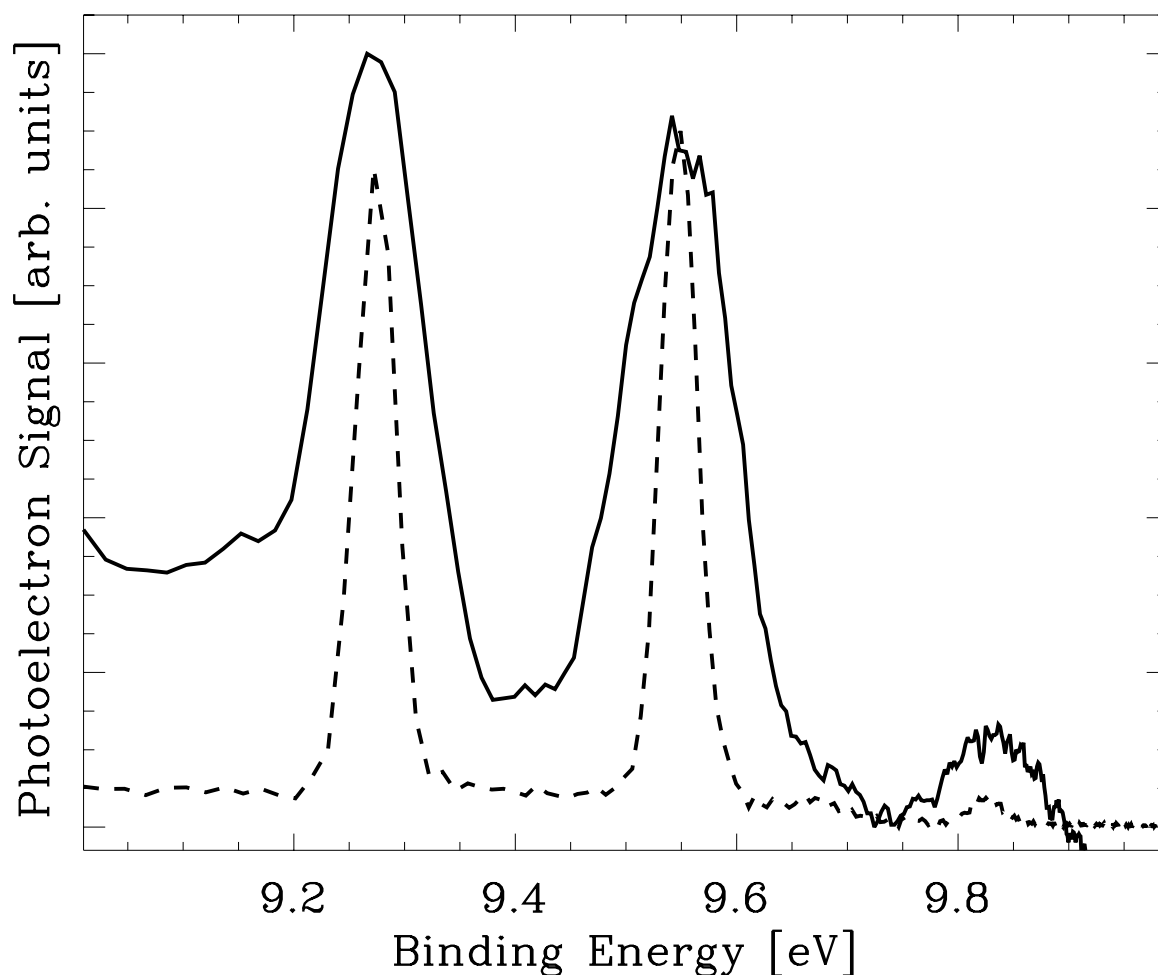


Figure 4.1: Photoelectron spectrum of NO gas taken with the 9th harmonic of a long pulse, narrowband Nd:YAG laser,  $E_{h\nu}=10.496$  eV (dashed line). Here the inherent resolution of the magnetic bottle spectrometer is seen in the peak widths. The vibrational progression of the  $\text{NO}^+$  ground state gives rise to the three peaks separated by  $\approx 0.28$  eV. The solid line shows the same vibrational progression, but acquired with the 7th harmonic (centered at  $E_{h\nu}=10.91$  eV) of the fs Ti:Sapphire laser. The broadening of the peaks is due to the energy bandwidth of the 7th harmonic. The height discrepancy in the highest binding energy peak between the Nd:YAG laser and the 7th harmonic of the Ti:Sapphire laser is due to the efficiency of the photoelectron spectrometer at different photoelectron energies. Though these peaks have the same binding energy, the dashed line peak at 9.8 eV corresponds to very low photoelectron energy, where the collection efficiency is quite low.

trometer broadening of 0.25 eV at a photoelectron energy of 5 eV. Therefore, for photoelectron peaks at energies beyond 5 eV, a broadening due to the energy bandwidth of the photon source that is less than 0.25 eV is masked by the spectrometer resolution. This means that unambiguous bandwidth information can only be extracted from low kinetic-energy photoelectron peaks. In this work two methods are therefore utilized. Specific atomic or molecular transitions that fortuitously yield low energy electrons for certain harmonics are studied in one series of measurements and the retarding grids are used to lower the electron energies in the other.

To obtain bandwidth measurements of the harmonics, photoelectron spectra of several atomic and molecular gases were taken, using either the specular reflection of the gratings or individual harmonics. From these photoelectron spectra, we measured photoelectron peaks resulting from ionization of a number of different harmonics. First, by using several different target gases, it is possible to obtain low energy photoelectron peaks directly resulting from ionization with a range of harmonics. Each atom or molecule has a characteristic ionization potential and precise core-level binding energies.

In addition to Xe (see Fig. 3.5, chapter 3), photoelectron spectra of Ne, Ar, and Kr were also taken. Similar to Xe, the main ionization peaks of these other rare gases exhibit a doublet structure due to the spin-orbit splitting of the ionic ground state. This splitting is too small in the cases of Ne and Ar to be fully resolved and the corresponding peaks were not used for bandwidth measurements. Ionization of rare gases from *ns* levels, on the other hand, does not suffer from spin orbit splitting, but the cross sections are generally small. This ionization process was only observed in the case of Ne.

Photoelectron spectroscopy of molecular gases with the harmonics is also possible, and several peaks from N<sub>2</sub> and NO were measured. The peaks from NO, shown as the solid line in Fig. 4.1, are especially important, since they represent the same vibrational progression that was obtained with the narrow band Nd:YAG laser, except using the 7th harmonic of the Ti:Sapphire laser. Comparison of the two spectra in Fig. 4.1 clearly shows the broadening of the photoelectron peaks due to the bandwidth of the 7th harmonic.

Using all the data discussed above from He, Kr, Xe, N<sub>2</sub>, and NO, we measured the full-width at half maximum of several photoelectron peaks with energies ranging from 1-20 eV. In Fig. 4.2, a plot of  $\Delta E_{pe}/E_{pe}$  vs. photoelectron energy,  $E_{pe}$ , is shown. From this figure two different trends in measured bandwidth can be seen. The high kinetic energy photoelectron peaks converge to a value around 5% which is due to the spectrometer resolution, and the peaks below  $\approx 4$  eV photoelectron kinetic energy show a steep rise, where the bandwidth is primarily due to the energy width of the harmonic light used to eject that electron. We then take the points below 4 eV in Fig. 4.2 and, after deconvolution with the spectrometer width, plot  $\Delta E_{pe}$  (now equal to  $\Delta E_{h\nu}$ ) as a function of photon energy,  $E_{h\nu}$ , in Fig. 4.3(a). All the points in Fig. 4.3(a) were taken without the use of the retarding grids.

A more complete study was done, however, by utilizing the retarding grids in the magnetic bottle system. In this way, a particular transition (for example, the main ionization peak of He) can be selected, and the electron kinetic energy is shifted into the region where the bandwidth of the laser dominates the spectrometer width for each harmonic (under 3 eV photoelectron kinetic energy after deceleration). Fig. 4.3b shows  $\Delta E_{h\nu}$  vs.  $E_{h\nu}$  for the measured bandwidths of all harmonics from the 9th to the 55th using the main ionization line in He and the  $\text{Xe} \rightarrow \text{Xe}^+(5p_{3/2})$  and  $\text{Xe} \rightarrow \text{Xe}^+(4d_{5/2})$  transitions. It can be seen from comparison of the two plots in Fig. 4.3 that the general trend is very similar, which gives confirmation that any broadening effect of the retarding grids can be ruled out. A list of the average  $\Delta E_{h\nu}$  values for harmonics 9-55 is given in Table 4.

In Fig. 4.2, the natural widths of the Xe 4d core level peaks are taken into account. Core level ionization results in an ionic core hole state that decays very rapidly via Auger processes. Hence, core level photoelectron peaks may exhibit a significant natural linewidth. The width of the Xe 4d levels has been the subject of several previous investigations, which report widths between 0.10 and 0.12 eV [50, 51]. The measured widths of the Xe 4d peaks in Fig. 4.3 and Table 4 are corrected for both the spectrometer broadening and the natural linewidth.

Another source of chirp and thus temporal broadening of the high harmonics stems from

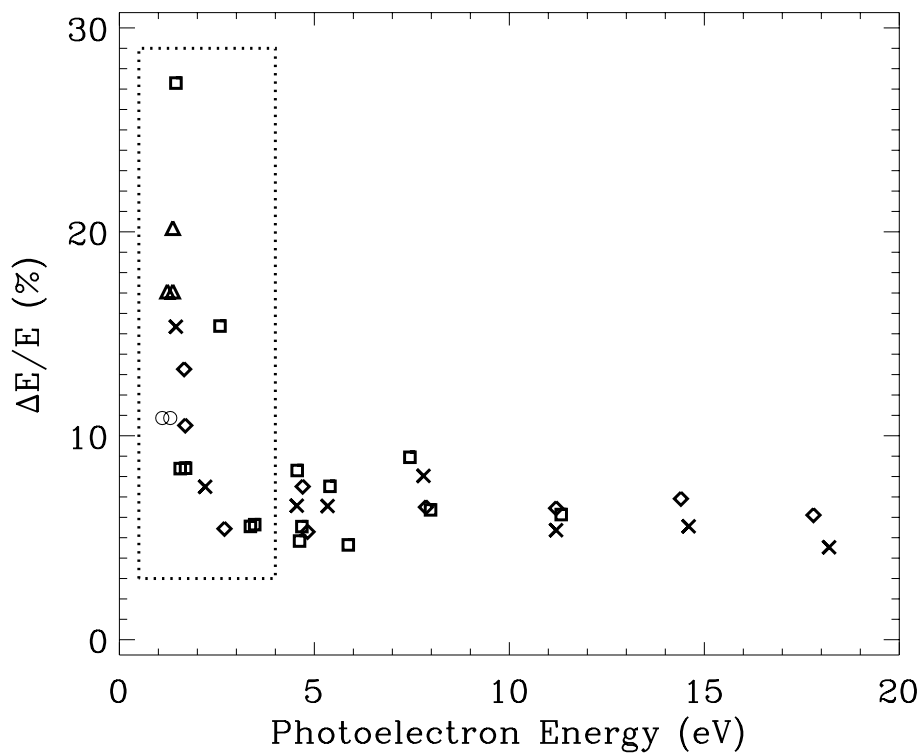


Figure 4.2: The relative energy width of photoelectron peaks from several different gases vs. their respective photoelectron energies. The higher energy photoelectron peaks converge to a relative width of 4-5%. For photoelectron peaks below  $\approx 4$  eV a new trend can be seen, where the  $\Delta E$  of the peaks is due to the energy bandwidth of the harmonics. Target gas is He ( $\diamond$ ), Ne ( $\times$ ), Xe ( $\square$ ), N<sub>2</sub> ( $\triangle$ ), and NO ( $\circ$ ).

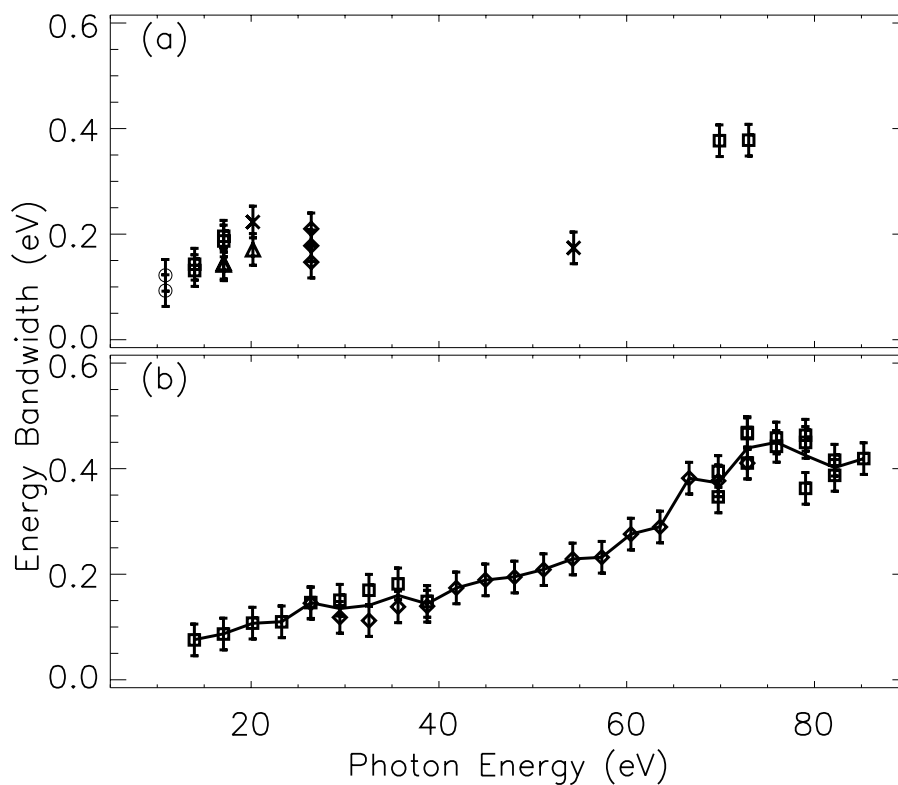


Figure 4.3: (a) The absolute energy width of the harmonics derived from low energy photoelectron peaks (below 3 eV) are plotted as a function of the photon energy, or the harmonic used to ionize the electron from which the peak arises. The retarding grids in the electron flight tube were not used for this data set. (b) A more complete data set using the retarding grids to measure the bandwidths of all the harmonics from the 9th to the 55th. Comparison of (a) and (b) shows that no artificial broadening exists when utilizing the retarding grids. Target gases are He ( $\diamond$ ), Ne ( $\times$ ), Xe ( $\square$ ),  $N_2$  ( $\triangle$ ), and NO ( $\circ$ ), and the solid line is the average for each harmonic.

Harmonic	$\Delta E$ (eV)	Harmonic	$\Delta E$ (eV)
7	0.11	33	0.21
9	0.08	35	0.23
11	0.09	37	0.22
13	0.10	39	0.28
15	0.11	41	0.29
17	0.15	43	0.38
19	0.14	45	0.37
21	0.14	47	0.44
23	0.16	49	0.45
25	0.14	51	0.43
27	0.17	53	0.40
29	0.19	55	0.42
31	0.20		

Table 4.1: Energy bandwidths for harmonics 7-55 generated in neon

the harmonic generation process itself. It has been reported that an unchirped driving pulse produces negatively chirped harmonics and that the best high harmonic generation is achieved if the driving pulse is slightly positively chirped [52]. We have investigated the effect of a chirped fundamental pulse on the high harmonic photoelectron spectra for both positive and negative chirps of up to 0.3 nm/fs. While for small positive chirps of  $\approx 0.1$  nm/fs the harmonic generation efficiency is slightly improved compared to an unchirped driving pulse, the efficiency drops off strongly for more positively and for negatively chirped pulses. The measured bandwidths, however, remain constant except for large negative chirps where a broadening of about a factor of 1.5 was observed. A demonstration of this is seen in Fig. 4.4, where photoelectron spectra of NO with both the 7th and the 9th harmonic are shown. Very little broadening in the photoelectron spectra can be seen between spectra with an unchirped, negatively chirped or positively chirped pulse, in contrast to the results from ref. [52] where chirping the 10 fs driving pulse gave either discrete harmonics (negative chirp) or a continuum (positive chirp). Though no broadening effects are observed, small energy shifts in the spectrum indicate the center wavelength of the harmonic is effected as the fundamental laser chirp is varied. This could be due to a change

in the wavelength of the fundamental laser.

In one experiment with similar conditions to the system here, a narrow slit monochromator is used to scan through the 27th harmonic of a 140 fs Cr:LiSAF laser. The energy bandwidth of the 27th harmonic is found to be  $\approx 0.12$  eV [53]. This agrees well with the result from this work (0.17 eV for the 27th harmonic), because a slightly larger energy bandwidth is expected here corresponding to our shorter pulse length. In another experiment, the 7th and 9th harmonics of a 100 fs Ti:Sapphire laser are measured to have a FWHM of  $\approx 0.1$  eV [40], also consistent with the measurements here. Measured bandwidths of harmonics generated by picosecond lasers, such as in Ref. [54], are quite narrow and cannot be compared directly to the results found here. Though other harmonic spectra are reported throughout the literature [20, 21, 41, 55], bandwidth measurements are not discussed and are not easily derived from the figures.

The general trend seen in Fig. 4.3 is a gradually increasing bandwidth from the 7th harmonic to the 45th harmonic, from  $0.11(\pm 0.03)$  eV to  $0.37(\pm 0.03)$  eV. The higher harmonics, from the 47th-55th, seem to reach a plateau centered around 0.43 eV. Theoretical treatments of spectral width vs. harmonic number do exist for driving laser pulses  $\leq 30$  fs [25, 26]. Comparison of the results reported here and these theoretical predictions is difficult for several reasons. First, for longer driving laser pulses, theory becomes increasingly difficult as more optical cycles must be treated numerically. Second, for very short pulses, saturation due to ionization of the non-linear gas medium is not reached, since the response time of the atoms is slow compared to the temporal envelope of the pulse. In the case of longer pulses, however, saturation is reached somewhere after the peak of the pulse on the falling edge. Nevertheless, we believe it is beneficial to mention the results of theoretical calculations and draw comparisons where it is appropriate.

According to calculations in the single atom picture of harmonic generation from short pulses, the phase structure of the generated harmonics plays a significant role [25]. A simple quadratic phase structure gives rise to linear chirp in the pulse, and no broadening of the spec-

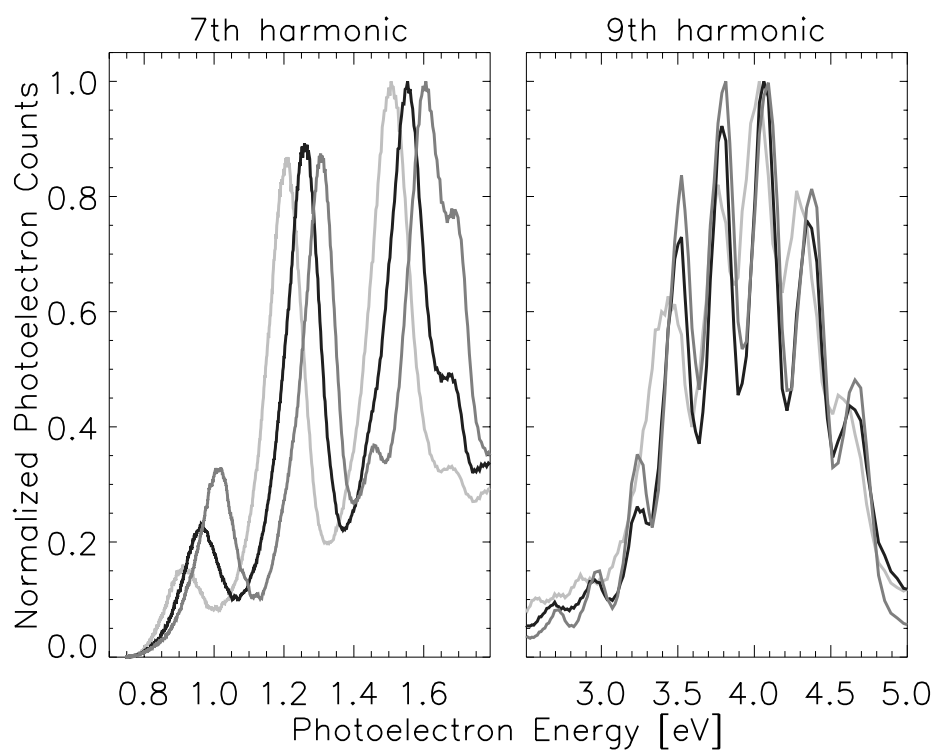


Figure 4.4: The photoelectron spectrum of NO gas with the 7th harmonic (left) and 9th harmonic (right), showing the vibrational progression of the  $\text{NO}^+$  ground state. The black spectrum represents the 70 fs unchirped pulse, while the light gray spectrum is taken with a positively chirped driving pulse and the dark gray spectrum is taken with a negatively chirped pulse.

trum within the pulse occurs. On the other hand, a complex phase structure with higher order terms leads to non-linear chirp and thus broadening of the spectrum through the introduction of new spectral components. The phase of the generated harmonics is said to be dependent on the intensity variation of the driving pulse, which changes dramatically during harmonic generation for a very short pulse. In this single atom picture, the lower and mid range harmonics have a complex phase structure, due to the fact that these harmonics are created over a larger number of optical cycles, with contributions from the rising edge, the peak, and the falling edge of the pulse. The higher harmonics near the cutoff, however, are created over the few optical cycles near the peak of the pulse, giving rise to a simple quadratic phase structure. This leads to a calculated harmonic spectrum with broad, unresolved lower harmonics and well resolved harmonics near the cutoff.

However, when the macroscopic conditions of harmonic generation are considered in addition to the single atom response, the results can be much different. In ref. [26], several aspects of the bulk medium are considered, such as phase matching and the focus position of the laser with respect to the gas jet. They give a two trajectory picture of harmonic generation, where the ionized electron can return to the ion on a short or long trajectory. These two trajectories can interfere with each other, or one can dominate depending on the conditions of harmonic generation. If the jet is located after the focus, the short return time is dominant, which results in a weak intensity dependence of the phase. This gives rise to a well-resolved spectrum with decreasing widths for decreasing harmonics orders. If the jet is at the focus, the calculated spectrum shows the opposite trend.

The argument that the high harmonics near the cutoff are created only near the peak of the driving pulse is expected to remain true for 70 fs pulses. Therefore, it could be argued that the plateau seen in Fig. 4.3(b) is due to this effect, namely that the harmonics in the cutoff region exhibit only a constant linear chirp and no further broadening is seen. It may seem that the two trajectory picture could account for the fact that we see a decreasing bandwidth with decreasing harmonic number but we do not observe any difference in the bandwidths of the high harmonics

when the position of the jet with respect to the focus is changed. We therefore conclude that a theoretical study based on the particular parameters of this experiment is needed to fully explain the observed bandwidth trends.